

## Chapter 1

## Half-Skym ion theory for high-temperature superconductivity

Takao Morihari

Yukawa Institute for Theoretical Physics, Kyoto University, Kyoto 606-8502,  
Japan

We review the half-Skym ion theory for copper-oxide high-temperature superconductivity. In the theory, doped holes create a half-Skym ion spin texture which is characterized by a topological charge. The formation of the half-Skym ion is described in the single hole doped system, and then the half-Skym ion excitation spectrum is compared with the angle-resolved photoemission spectroscopy results in the undoped system. Multi-half-Skym ion configurations are studied by numerical simulations. We show that half-Skym ions carry non-vanishing topological charge density below a critical hole doping concentration 30% even in the absence of antiferromagnetic long-range order. The magnetic structure factor exhibits incommensurate peaks in stripe ordered configurations of half-Skym ions and anti-half-Skym ions. The interaction mediated by half-Skym ions leads to  $d_{x^2-y^2}$ -wave superconductivity. We also describe pseudogap behavior arising from the excitation spectrum of a composite particle of a half-Skym ion and doped hole.

## 1.1. Introduction

One of the most challenging problems in condensed matter physics is to unveil the mechanism of high-temperature superconductivity in the copper oxides. Although it has past more than two decades since its discovery,<sup>1</sup> no established theory exists. The most difficult aspect is to cope with strong electron correlations: The undoped system of high-temperature superconductors is an insulator. Contrary to conventional band insulators, strong Coulomb repulsion makes the system insulating. High-temperature superconductivity occurs by doping holes in such a Mott insulator.<sup>2</sup> The pairing symmetry is not conventional s-wave but  $d_{x^2-y^2}$ -wave.<sup>3</sup> It is believed that electron-phonon couplings do not play an essential role in the mechanism of high-temperature superconductivity because of the strong Coulomb repulsion. Searching for a mechanism based on the strong electron correlation is necessary. In this chapter, as a candidate providing such a mechanism the half-Skym ion theory is reviewed.

The plan of the review is as follows. In Sec. 1.2, we review the structure,

electronic properties, and the phase diagram of high-temperature superconductors. Then, we describe the half-Skym ion spin texture in a single hole doped system in Sec. 1.3. The half-Skym ion excitation spectrum is compared with the angle-resolved photoemission spectroscopy results in the undoped system. Topological character and magnetic properties of multi-half-Skym ion configurations are described in Sec. 1.4. In Sec. 1.5, we describe a mechanism of  $d_{x^2-y^2}$ -wave superconductivity based on half-Skym ions. In Sec. 1.6, we describe a pseudogap behavior in the half-Skym ion system. It is shown that the energy dispersion of a composite particle of a half-Skym ion and doped hole leads to an arc-like Fermi surface.

## 1.2. Review of high-temperature superconductivity

Although there are a number of high-temperature superconductors, the essential structure is the  $\text{CuO}_2$  plane. Material differences arise from an insulating layer sandwiched by  $\text{CuO}_2$  planes.<sup>2</sup> In the parent compound, nine electrons occupy 3d orbitals at each copper ion. In the hole picture, there is one hole at each copper site. The hole band is half-filled but the system is an insulator because of a strong Coulomb repulsion. The system is well described by the spin  $S = 1/2$  antiferromagnetic Heisenberg model on the square lattice with the superexchange interaction  $J \sim 1500\text{K}$ .<sup>4</sup> Experimentally and theoretically it is established that the ground state is an antiferromagnetic long-range ordered state.<sup>4</sup> The structure of the  $\text{CuO}_2$  plane and the arrangement of spins at copper sites in the undoped system are schematically shown in Fig. 1.1 (a).

This antiferromagnetic long-range order is rapidly suppressed by hole doping. In fact only 2–3% doping concentration is enough to kill antiferromagnetic long-range order. This critical hole concentration is much lower than the percolation limit of 40%. High-temperature superconductivity occurs by introducing about 0.05 holes per copper ion. A schematic phase diagram is shown in Fig. 1.1 (b). (In this review we focus on the hole doped system and do not discuss the electron doped system.)

In the high-temperature superconductors anomalous behaviors are observed in physical quantities for temperatures above the superconducting transition temperature,  $T_c$ .<sup>5</sup> The phenomenon is called pseudogap. The Fermi surface observed by angle-resolved photoemission spectroscopy (ARPES) in the underdoped regime is a truncated, arc-like Fermi surface.<sup>6</sup> (See for a review, Ref. 7.) In scanning tunneling spectroscopy, a gap-like feature appears below the pseudogap temperature  $T^*$  which is higher than  $T_c$ .<sup>8</sup> For temperatures below  $T^*$  gap-like behaviors are observed in NMR, transport coefficients, and optical conductivity. (See for a review, Ref. 5.)

In the doped system, because of the strong Coulomb repulsion at each copper site<sup>2</sup> doped holes occupy oxygen p-orbitals. Hole spins interact with copper site spins with strong antiferromagnetic Kondo interaction. Because Kondo interaction coupling,  $J_K$ , is much larger than  $J$  and hole hopping matrix elements, there is

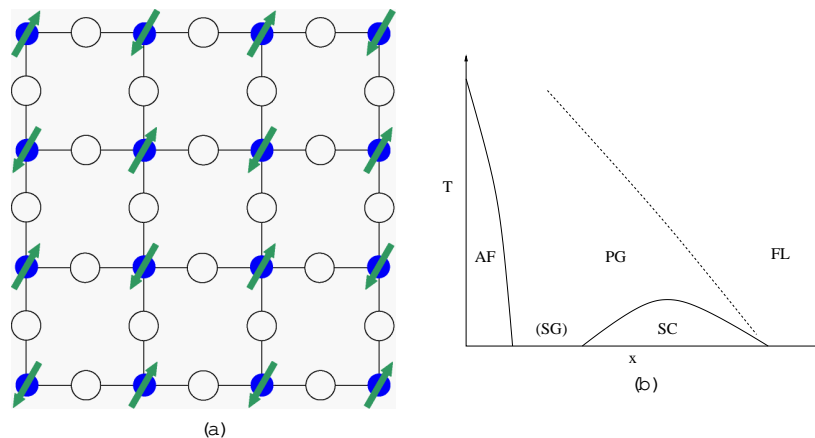


Fig. 1.1. (a) Two-dimensional  $\text{CuO}_2$  plane. Filled circles represent copper ions. Open circles represent oxygen ions. Arrows are localized spin moments at each copper site. In the ground state, those spins have anti-ferromagnetic long-range order. (b) A schematic phase diagram of the high-temperature superconductors. The horizontal axis represents the doped hole concentration and the vertical axis represents temperature. AF indicates antiferromagnetic long-range order and SC indicates superconductivity. Below a characteristic temperature curve denoted by the dashed line, the system shows a pseudogap behavior (denoted by PG). SG and FL indicate spin-glass-like state and Fermi liquid state, respectively.

correlation of forming a singlet pair called the Zhang-Rice singlet.<sup>9</sup>

The strong  $J_K$  limit leads to the  $t$ - $J$  model.<sup>9</sup> The  $t$ - $J$  model has been studied extensively. (See for a review, Ref. 10.) In the  $t$ - $J$  model, double occupancy is projected out. One way to deal with this constraint is to use slave-particle formulations. Based on the resonating valence bond picture proposed by Anderson,<sup>11</sup> a spin-charge separation scenario has been applied to the physics of high-temperature superconductors.<sup>10</sup> From various physical viewpoints different theories have been proposed. There is a view in which incommensurate spin correlations observed in neutron scattering are associated with stripe order. (See for a review, Ref. 12.) Chakravarty et al. proposed d-density wave order as competing order against superconductivity to explain the pseudogap phenomenon.<sup>13</sup> The half-Skyrmion theory has some connection with these theories which will be discussed later.

### 1.3. Single hole doped system

The high-temperature superconductors are characterized by a rich phase diagram shown in Fig. 1.1(b). Remarkably this phase diagram is essentially controlled by a single parameter  $x$ , the doped hole concentration. Therefore, to understand the physics of high-temperature superconductivity it is necessary to establish how to describe doped holes. Here we consider a half-Skyrmion spin texture created by a doped hole in an antiferromagnetically correlated spins.

As the simplest model we consider the single hole doped system. As stated in the previous section, the undoped system is described by the antiferromagnetic Heisenberg model on the square lattice,

$$H = J \sum_{\langle i,j \rangle} \mathbf{S}_i \cdot \mathbf{S}_j; \quad (1.1)$$

where the summation is taken over the nearest neighbor sites and the vector  $\mathbf{S}_i$  describes a spin  $S = 1/2$  at site  $i$ . Theoretically and experimentally it has been established that the ground state is the antiferromagnetic long-range ordered state.<sup>4</sup> A convenient description of the state is obtained by introducing Schwinger bosons<sup>14</sup> and then describing the long-range ordered state in terms of a Bose-Einstein condensate of those Schwinger bosons. In the Schwinger boson theory the spin  $\mathbf{S}_i$  is represented by

$$\mathbf{S}_i = \frac{1}{2} \sum_{\alpha, \beta} \mathbf{b}_{i\alpha}^\dagger \mathbf{b}_{i\beta} \boldsymbol{\sigma}_{\alpha\beta};$$

where the components of the vector  $\boldsymbol{\sigma} = (\sigma_x; \sigma_y; \sigma_z)$  are Pauli spin matrices. To describe the spin  $S = 1/2$ , the Schwinger bosons must satisfy the constraint,  $\sum_{\alpha} \mathbf{b}_{i\alpha}^\dagger \mathbf{b}_{i\alpha} = 1$ . We introduce a mean field  $A_{ij} = \langle \mathbf{b}_{i\alpha}^\dagger \mathbf{b}_{j\alpha} \rangle$  and introduce a Lagrange multiplier  $\lambda_j$  to impose the constraint. In the Schwinger boson mean field theory,<sup>14</sup> we assume uniform values for these quantities as  $A_{ij} = A$  and  $\lambda_j = \lambda$ . The energy dispersion of Schwinger bosons is given by  $\epsilon_k = \frac{2JA}{2 - 4J^2 A^2} \omega_k$  with  $\omega_k = (\sin k_x + \sin k_y)/2$ . In the ground state,  $\lambda = 2JA$ . Bose-Einstein condensation occurs<sup>15(17)</sup> at  $k = (0, 0)$ .

Now we consider a hole introduced in the system. The strong interaction between the doped hole spin and copper site spins leads to correlation of forming a Zhang-Rice spin singlet<sup>9</sup> as mentioned in the previous section. If the singlet is formed, then the Bose-Einstein condensate of the Schwinger bosons is suppressed around the doped hole position. Generally if the condensate is suppressed at some point in two-dimensional space, then a vortex is formed around that point. The vortex solution is found by solving the Gross-Pitaevskii equation.<sup>18</sup> For the Schwinger bosons, the vortex turns out to be a half-Skyrmion as shown below.

For the description of the half-Skyrmion, it is convenient to use the non-linear sigma model.<sup>19</sup> Low-energy physics of the antiferromagnetic Heisenberg model is well described by the non-linear sigma model,<sup>19</sup>

$$S = \frac{s}{2} \int d^2r \left[ \frac{1}{c_{sw}^2} \left( \frac{\partial \mathbf{n}}{\partial t} \right)^2 + (\nabla \mathbf{n})^2 \right]; \quad (1.2)$$

where  $s$  is the spin stiffness and  $c_{sw}$  is the antiferromagnetic spin-wave velocity. (Hereafter we use units in which  $\hbar = 1$ .) The unit vector  $\mathbf{n}$  represents the staggered moment and  $t$  is the imaginary time.

In order to describe the correlation of forming a Zhang-Rice singlet pair between doped hole spins and copper site spins, one has to be careful about its description.

Obviously forming a static singlet state which is realized in the  $J_K \rightarrow 1$  limit does not work. Because such a simple singlet state contradicts with the rapid suppression of antiferromagnetic long-range order by hole doping. If static singlet states are formed, then sites occupied by singlets do not interact with the other spins at all. The situation is similar to site dilution, and suppression of magnetic long-range order is described by the percolation theory. In other words, considering a strongly localized wave function of a doped hole at a copper site is not realistic. We need to consider a hole wave function extending over some area so that the doped hole spin interacts with the other spins. In fact, numerical diagonalization studies of the  $t$ - $J$  model show a Skyrmion-like spin texture<sup>20</sup> when a hole motion is restricted to one plaquette. A similar situation may be realized in Li-doped system as discussed in Ref. 21.

To include the effect of the interaction with the other spins, we formulate the correlation of forming a Zhang-Rice singlet in the following way. The spin singlet wave function of a copper site spin and a hole spin is described by

$$\frac{1}{\sqrt{2}} (\uparrow i_h \downarrow i_{Cu} - \downarrow i_h \uparrow i_{Cu}) :$$

This wave function has the form of superposition of the hole spin-up and copper spin-down state,  $\uparrow i_h \downarrow i_{Cu}$  and the hole spin-down and copper spin-up state,  $\downarrow i_h \uparrow i_{Cu}$ . In order to include the interaction effect, we consider these states separately and construct superposition of them. We assume that the spin state at site  $j$  is spin-up before the introduction of a doped hole. Under this assumption, the spin-up state does not change directions of the neighboring spins. So the system is uniform for the staggered spin. By contrast, the spin-down state at site  $j$  creates a Skyrmion spin texture characterized by a topological charge,

$$Q = \frac{1}{8} \int_Z d^2r [\partial_x n - \partial_y n - (\partial_x n + \partial_y n)^2] ;$$

where  $\partial_{xx} = \partial_{yy} = 0$  and  $\partial_{xy} = -\partial_{yx} = 1$ . Following Ref. 22, the Skyrmion solution is found by making use of an inequality

$$\int_Z d^2r [\partial_x n - \partial_y n - (\partial_x n + \partial_y n)^2] \geq 0 :$$

The classical energy satisfies,

$$E = \frac{s}{2} \int_Z d^2r (r n)^2 - 4 s Q :$$

The equality holds if and only if

$$\partial_x n - \partial_y n - (\partial_x n + \partial_y n)^2 = 0 : \quad (1.3)$$

This equation is rewritten in a simple form. If we introduce

$$w = \frac{n_x + i n_y}{1 - n_z} ;$$

then Eq. (1.3) is rewritten as

$$(\partial_x - i\partial_y)w = 0:$$

This equation is the Cauchy-Riemann equation. Noting

$$n = \frac{2\text{Re}w}{|w|^2 + 1}; \frac{2\text{Im}w}{|w|^2 + 1}; \frac{|w|^2 - 1}{|w|^2 + 1};$$

the solutions satisfying the boundary condition  $n(r_j) = \hat{z}$  and  $n(r \rightarrow \infty) = \hat{z}$  with  $\hat{z}$  the unit vector along the z-axis are the Skyrme spin texture,

$$n(r) = \frac{2x}{r^2 + 2}; \frac{2y}{r^2 + 2}; \frac{r^2 - 2}{r^2 + 2};$$

with  $Q = 1$  and the anti-Skyrme spin texture,

$$n(r) = \frac{2x}{r^2 + 2}; \frac{2y}{r^2 + 2}; \frac{r^2 - 2}{r^2 + 2};$$

with  $Q = -1$ .

Now we consider superposition of the uniform state and the Skyrme state. Although superposition of the two spin configurations is not the solution of the field equation, these solutions suggest that the resulting spin configuration is characterized by a topological charge  $Q$  with  $0 < |Q| < 1$ . The value of  $Q$  is determined by making use of the fact that the antiferromagnetic long-range ordered state is described by Bose-Einstein condensation of Schwinger bosons. In the  $CP^1$  representation of the non-linear sigma model,<sup>23</sup> the  $U(1)$  gauge field is introduced by

$$X = i \int d^2z \partial_z \bar{z} \partial_{\bar{z}} z \quad (1.4)$$

where the complex field  $z$  is defined through

$$n = \frac{z_{\bar{z}} z_z - z_z z_{\bar{z}}}{z_{\bar{z}} z_z + z_z z_{\bar{z}}}: \quad (1.5)$$

In terms of the gauge field, the topological charge  $Q$  is rewritten as

$$Q = \frac{1}{2\pi} \int d^2r (\partial_x \bar{y} - \partial_y \bar{x}):$$

From this expression, we see that a spin configuration with  $Q$  corresponds to the flux  $2\pi Q$  in the condensate of the Schwinger bosons. On the other hand, each Schwinger boson carries the spin  $S = 1/2$ . However, there are no  $S = 1/2$  excitations in the low-energy excitation spectrum. Low-lying excitations are antiferromagnetic spin waves which carry the spin one. Therefore, all Schwinger bosons are paired and the flux quantum is similarly to conventional BCS superconductors.<sup>24</sup> The flux value is not arbitrary and  $Q$  must be in the form of  $Q = n/2$ , with  $n$  an integer. Taking into account the constraint  $0 < |Q| < 1$ , we may conclude  $|Q| = 1/2$ .<sup>25</sup> The spin texture with  $|Q| = 1/2$  is called half-Skyrme spin texture because the topological

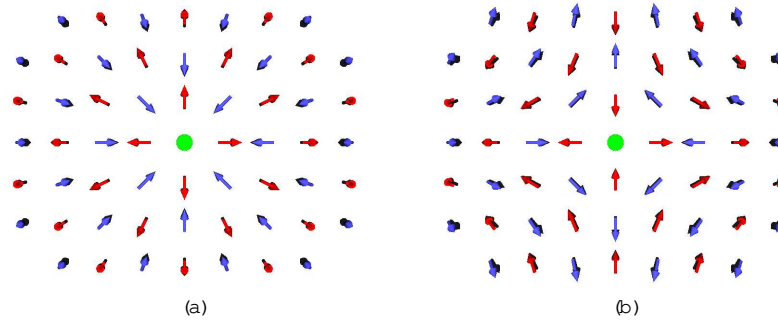


Fig.1.2. (a) Half-Skyrmion spin texture. Arrows represent the directions of the spin at the copper sites. Neighboring spins are almost anti-parallel because of the antiferromagnetic correlations. Filled circle at the center denotes the core of the half-Skyrmion. (b) Anti-half-Skyrmion spin texture.

charge is half of the Skyrmion spin texture. The half-Skyrmion spin texture and the anti-half-Skyrmion spin texture are schematically shown in Fig.1.2.

Moving half-Skyrmion spin texture is obtained by applying Lorentz boost on the static solution above by making use of the Lorentz invariance of the non-linear sigma model.<sup>23</sup> The energy dispersion is

$$E_k = \frac{q}{c_{sw}^2} k^2 + E_0^2; \quad (1.6)$$

where  $E_0 = 2\epsilon_s$  is the half-Skyrmion creation energy. On the square lattice the dispersion is transformed into

$$E_k = \frac{q}{c_{sw}^2} (\cos^2 k_x + \cos^2 k_y) + E_0^2; \quad (1.7)$$

Note that the lowest energy states are at  $(\pi, \pi)$  because the Schwinger bosons are gapless at those points in the antiferromagnetic long-range ordered state. The half-Skyrmion spin texture are mainly formed by Schwinger bosons around those points.

Now we compare the half-Skyrmion excitation spectrum with the ARPES result in the undoped system. The excitation spectrum Eq. (1.7) is qualitatively in good agreement with excitation spectrum obtained by Wells et al.<sup>26</sup> The parameters  $c_{sw}$  and  $E_0$  are determined from the values for the Heisenberg antiferromagnet. We use the renormalized factors  $Zc = 1.17$  and  $Z\epsilon_s = 0.72$ , which are estimated from quantum Monte Carlo simulations<sup>27,28</sup> and a series expansion technique.<sup>29</sup> Using these values, we find that the bandwidth is 1.5J and  $E_0 = 1.1J$ . The experimentally estimated bandwidth by Wells et al. is 2.2J. From the fitting of the experimental data assuming Eq. (1.7), we find  $E_0 = 1J$ .

In the undoped system, anomalously broad line shapes are observed by ARPES. Line shape broadening is associated with scattering of excitations by fluctuation modes. In the half-Skyrmion theory, half-Skyrmions couple to spin-wave excitations. Describing those spin-wave excitations in terms of the gauge field fluctuations line

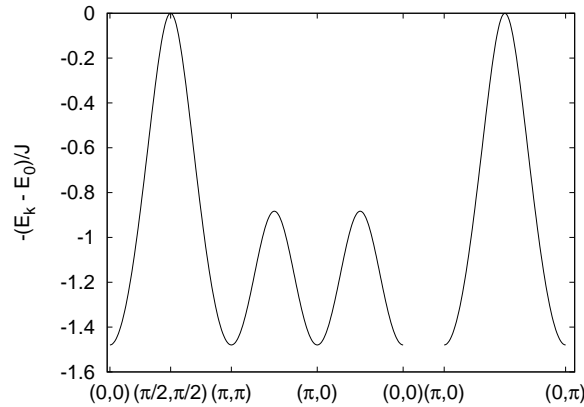


Fig. 1.3. The half-Skyrmion dispersion. Horizontal axis represents positions in the Brillouin zone.

shape broadening is studied by applying a strong coupling analysis.<sup>30</sup> The width of the broadening is in good agreement with the experiment.

#### 1.4. Multi-half-Skyrmion configurations

In the previous section, the single half-Skyrmion has been considered. The most important physical quantity carried by the half-Skyrmion is the topological charge. The topological charge density, which is defined in the continuum as

$$q_z(\mathbf{r}) = \frac{1}{4} n(\mathbf{r}) [\partial_x n(\mathbf{r}) \partial_y n(\mathbf{r})];$$

has the following form on the lattice,

$$q_z(\mathbf{x}_j; \mathbf{y}_j) = \frac{1}{16} n(\mathbf{x}_j; \mathbf{y}_j) [n(\mathbf{x}_j + 1; \mathbf{y}_j) - n(\mathbf{x}_j - 1; \mathbf{y}_j)] [n(\mathbf{x}_j; \mathbf{y}_j + 1) - n(\mathbf{x}_j; \mathbf{y}_j - 1)]:$$

In the single half-Skyrmion state,  $q_z(\mathbf{x}_j; \mathbf{y}_j)$  has a peak around the half-Skyrmion position, and vanishes at infinity. The integration of  $q_z(\mathbf{r})$  leads to the quantized value  $Q = \pm 1/2$ .

If there are many half-Skyrmions, do half-Skyrmions keep topological charge? In order to answer this question, we carry out a simple numerical simulation. First, we put either an XY-spin-vortex or an anti-XY-spin-vortex randomly. (A similar numerical simulation is discussed in Ref. 31.) A multi-XY-spin-vortex configuration is defined by

$$n_x(\mathbf{r}) = \sum_j^X q_j \frac{x - x_j}{(x - x_j)^2 + (y - y_j)^2}; \quad (1.8)$$

$$n_y(\mathbf{r}) = \sum_j^X q_j \frac{y - y_j}{(x - x_j)^2 + (y - y_j)^2}; \quad (1.9)$$



where  $q_j = +1$  for XY-spin-vortices and  $q_j = -1$  for anti-XY-spin-vortices. A doped hole is sitting at each spin-vortex position  $(x_j, y_j)$ , and  $n(x_j, y_j) = 0$ . Then, a random number which ranges from 0.1 to 0.1 is assigned to the z-component of the vector  $\mathbf{n}(x_i, y_i)$  except for the nearest neighbor sites  $(x_i - 1, y_i)$  and  $(x_i, y_i - 1)$ . After that, the equilibrium configuration of the vectors  $\mathbf{n}(x_i, y_i)$  is obtained by the relaxation method. At site  $(x, y)$ ,  $\mathbf{n}(x, y)$  is updated by

$$\mathbf{n}(x, y) = \frac{1}{4} [\mathbf{n}(x+1, y) + \mathbf{n}(x-1, y) + \mathbf{n}(x, y+1) + \mathbf{n}(x, y-1)]:$$

The constraint  $|\mathbf{n}(x, y)| = 1$  is imposed by taking the normalization after the update. This update procedure is carried out over all lattice sites except for the hole positions  $(x_j, y_j)$  and its nearest neighbor sites,  $(x_j - 1, y_j)$  and  $(x_j, y_j - 1)$ . The resulting converged state is an approximate state for a multi-half-Skyrmion-anti-half-Skyrmion configuration. As an example, Fig.1.4 shows the topological charge density distribution at the doping concentration  $x = 0.107$ . There are regions where topological charge density is non-zero. Positive (negative) topological charge density region is associated with half-Skyrmions (anti-half-Skyrmions). Non-vanishing distribution patterns are observed for  $x < x_c$  with  $x_c = 0.30$ . For  $x > x_c$ , half-Skyrmions and anti-half-Skyrmions are heavily overlapped. As a result, topological charges are cancelled out. Therefore, above  $x_c$  the topological nature of half-Skyrmions is lost. (For related discussions about the effect of thermally excited skyrmions and hole-induced skyrmions, see Refs. 32,33.)

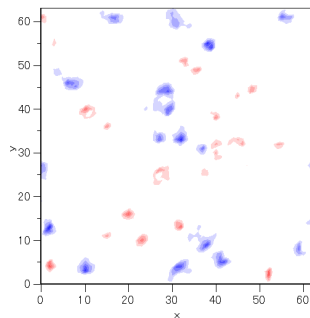


Fig. 1.4. Topological charge density distribution in real space at the doping concentration  $x = 0.107$  on a  $64 \times 64$  lattice. Positive values are shown in red and negative values are shown in blue.

Now we discuss magnetic properties of multi-half-Skyrmion configurations. The magnetic correlation is investigated by the static magnetic structure factor,

$$S(\mathbf{q}) = \frac{1}{N} \sum_{i,j} \frac{\mathbf{q}_i \cdot \mathbf{q}_j}{q^2} S_i S_j;$$

Here

$$S(\mathbf{q}) = \frac{1}{N} \sum_{i,j} e^{i\mathbf{q} \cdot (\mathbf{R}_i - \mathbf{R}_j)} S_i S_j :$$

$S(\mathbf{q})$  is measured by neutron scattering experiments. Introducing,

$$S(\mathbf{q}) = \sum_j e^{i\mathbf{q} \cdot \mathbf{R}_j} S_j;$$

$S(\mathbf{q})$  is rewritten as

$$S(\mathbf{q}) = \frac{1}{N} \sum_j S_j(\mathbf{q})^2 = \frac{1}{N} \sum_j S_j(\mathbf{q})^2;$$

If there is antiferromagnetic long-range order, then  $S(\mathbf{q})$  has a peak at  $\mathbf{q} = (\pi; \pi)$ , and the peak height is proportional to the number of lattice sites. From numerical simulations above, we find that  $S(\mathbf{q})$  shows incommensurate peaks at positions shifted from  $\mathbf{q} = \mathbf{Q}$ . Furthermore, we find that around  $x = 0.10$  the maximum peak height is on the order of the square root of the number of lattice sites. Therefore, the magnetic long-range order disappears around that doping concentration.

The physical origin of the incommensurate peaks is found by studying a regular configuration of half-Skyrmions. Taking a vortex-anti-vortex configuration given by  $q_{(x_j, y_j)} = (-1)^{x_j + y_j}$ , an approximate "antiferromagnetic" configuration of half-Skyrmions and anti-half-Skyrmions is obtained by the numerical simulation. Figure 1.5 (a) shows the magnetic structure factor of the resulting state at  $x = 0.0625$  on a  $64 \times 64$  lattice. The incommensurate peaks are found at  $(\pi/2; \pi/2)$  with  $\delta = 0.125$ . These peaks are associated with the superlattice formed by half-Skyrmions and anti-half-Skyrmions. A stripe order case is shown in 1.5 (b) which is obtained by taking a vortex-anti-vortex configuration with  $q_{(x_j, y_j)} = (-1)^{x_j}$ . The dominant incommensurate peaks are found at  $(\pi/2; \pi)$  with  $\delta = 0.125$ .

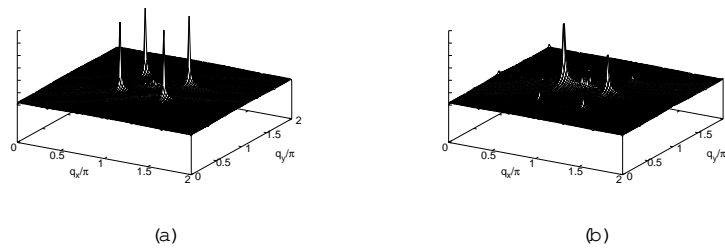


Fig.1.5. (a) Magnetic structure factor in a roughly antiferromagnetically ordered half-Skyrmions and anti-half-Skyrmions. (b) Magnetic structure factor in a stripe-like configuration of half-Skyrmions and anti-half-Skyrmions.

Experimentally neutron scattering experiments show incommensurate peaks at  $\mathbf{q} = (\pi/2; \pi/2)$  for  $x < 0.05$  and  $\mathbf{q} = (\pi/2; \pi)$  and  $\mathbf{q} = (\pi; \pi/2)$  for  $x > 0.05$ .<sup>34,36</sup> As shown above, such incommensurate peaks are found in some configurations of half-Skyrmions and anti-half-Skyrmions. However, there is a quantitative difference. Experimentally it is found that  $\delta \propto x$ .<sup>35,36</sup> In order to explain

this experimental result, it is necessary to consider stripe-like configurations of half-Skyrmions and anti-half-Skyrmions. To determine the stable configuration of half-Skyrmions and anti-half-Skyrmions, we need to take into account the interaction between half-Skyrmions, which is not included in the numerical simulation above. Determination of the stable half-Skyrmion configuration is left for future work.

### 1.5. Mechanism of d-wave superconductivity

In the half-Skyrmion theory, doped holes create either a half-Skyrmion or an anti-half-Skyrmion at their positions. A half-Skyrmion or an anti-half-Skyrmion is bound to each hole and moves together. There are two ways to formulate the effect of half-Skyrmions on the doped holes. One way is to take a doped hole and the half-Skyrmion created by the hole as a composite particle. This approach is formulated in the next section, and we shall see that the theory leads to pseudogap behavior.

The other way is to include the effect of half-Skyrmions as fields mediating interaction between doped holes. By integrating out the half-Skyrmion degrees of freedom, we obtain the interaction between doped holes mediated by the half-Skyrmions. In this section, we take this approach and show that the interaction leads to a  $d_{x^2-y^2}$ -wave Cooper pairing between the doped holes.<sup>37,38</sup> An intuitive interpretation is also given about the origin of the pairing interaction based on a Berry phase.

The fact that each doped hole carries a half-Skyrmion is represented by

$$\mathbf{r} = \sum_{s=\pm} \mathbf{s} \frac{Y}{s}(\mathbf{r}) \mathbf{s}(\mathbf{r}); \quad (1.10)$$

where  $\mathbf{s}$  is the  $U(1)$  gauge field in the  $CP^1$  model defined by Eq. (1.4). The index  $s$  labels the sign of the topological charge.  $s = +$  refers to a half-Skyrmion and  $s = -$  refers to an anti-half-Skyrmion.

The interaction between the doped hole current and the gauge field is found as follows. Doped holes interact with the spins via a strong Kondo coupling,

$$H_K = J_K \sum_j \mathbf{S}_j \cdot \mathbf{c}_j^\dagger \mathbf{c}_j;$$

Meanwhile, the doped hole motion is described by

$$H_t = t \sum_{\langle ij \rangle} c_i^\dagger c_j + h.c.;$$

From a perturbative calculation for the tight-binding model describing the  $CuO_2$  plane, we find the Kondo coupling is  $J_K \sim 1\text{eV}$ . Since  $J_K$  is larger than  $t \sim 0.4\text{eV}$ , we first diagonalize the Kondo coupling term. The diagonalization is carried out by the following unitary transformation,

$$c_j = U_j f_j;$$

where

$$U_j = \begin{pmatrix} Z_j'' & Z_j^\# \\ Z_j^\# & Z_j'' \end{pmatrix} :$$

Under this transformation, the hopping term is

$$H_t = -t \sum_{\langle i,j \rangle} f_i^y U_i^y U_j f_j + \text{h.c.} :$$

Extracting the terms including the gauge field, we find

$$H_{\text{int}} = it \sum_{j=x,y} \sum_{\langle j,j' \rangle} f_{j+}^y f_{j'} f_{j'} + \text{h.c.} :$$

(The effect of other terms is discussed in Ref.39.) After Fourier transforming and taking the continuum limit, we obtain

$$H_{\text{int}}' = \frac{1}{m} \sum_{k,q} \sum_{x,y} (q) \left( k + \frac{q}{2} \right) f_{k+q}^y f_k : \quad (1.11)$$

Here the effective mass  $m$  is introduced by  $t' = 2m$ .

Now we derive the pairing interaction between the doped holes from Eqs. (1.10) and (1.11) by eliminating the gauge field. In order to fix the gauge, we take the Coulomb gauge. In wavevector space, we set  $\epsilon_x(q) = \frac{iq_y}{q^2}(q)$  and  $\epsilon_y(q) = \frac{iq_x}{q^2}(q)$ . From Eq. (1.10), we obtain

$$(q) = \sum_{k,s} \frac{1}{1+2} s f_{k,s}^y f_{k+q,s} :$$

Substituting this expression into Eq. (1.11), we obtain

$$H_{\text{int}}' = \frac{i}{m} \sum_{k,k^0;q,s;s^0} \sum_{\langle k,k^0 \rangle} \frac{k_x q_y - k_y q_x}{q^2} s^0 f_{k^0,s^0}^y f_{k^0+q,s^0} f_{k+q,s}^y f_{k,s} :$$

Since we are interested in a Cooper pairing, we focus on terms with  $k + k^0 + q = 0$ . After symmetrizing the terms with respect to spin and half-Skyrmion indices, we obtain

$$H_{\text{int}}' = \frac{i}{m} \sum_{k \in k^0,s;s^0} \sum_{\langle k,k^0 \rangle} \frac{k_x k_y^0 - k_y k_x^0}{(k - k^0)^2} (s^0 + s^0) f_{k^0,s^0}^y f_{k^0,s}^y f_{k,s} f_{k;s^0} : \quad (1.12)$$

This interaction term leads to a pairing of holes as shown below.

Following a standard procedure,<sup>40</sup> we apply the BCS mean field theory to the interaction (1.12). The mean field Hamiltonian reads,

$$H = \sum_{\mathbf{k};s} \begin{pmatrix} f_{\mathbf{k};s}^y & f_{\mathbf{k};s}^y \\ 0 & 0 \end{pmatrix} \begin{pmatrix} (+) & (-) \\ (-) & (+) \end{pmatrix} \begin{pmatrix} 1 & 0 \\ 0 & 1 \end{pmatrix} \begin{pmatrix} f_{\mathbf{k};s} & f_{\mathbf{k};s}^y \\ f_{\mathbf{k};s}^y & 0 \end{pmatrix} \begin{pmatrix} C & B \\ C & B \\ A & A \end{pmatrix}; \quad (1.13)$$

The mean fields are defined by

$$\begin{pmatrix} (+) \\ \mathbf{k};s \end{pmatrix} = + \frac{2i}{m} \sum_{\mathbf{k} \neq \mathbf{k}^0} \frac{k_x k_y^0 - k_y k_x^0}{(k - k^0)^2} \hbar f_{\mathbf{k}^0;s} f_{\mathbf{k};s}; \quad (1.14)$$

$$\begin{pmatrix} (-) \\ \mathbf{k};s \end{pmatrix} = \frac{2i}{m} \sum_{\mathbf{k} \neq \mathbf{k}^0} \frac{k_x k_y^0 - k_y k_x^0}{(k - k^0)^2} \hbar f_{\mathbf{k}^0;-s} f_{\mathbf{k};s}; \quad (1.15)$$

The mean field (1.14) is associated with the Cooper pairing between holes with the same spin and the same half-Skyrmion index. On the other hand, the mean field (1.15) is associated with the Cooper pairing between holes with the opposite spin and the opposite half-Skyrmion index.

If we consider the interaction (1.12) only, then the pairing states described by  $\begin{pmatrix} (+) \\ \mathbf{k};s \end{pmatrix}$  and  $\begin{pmatrix} (-) \\ \mathbf{k};s \end{pmatrix}$  are degenerate energetically. However, if we include the (anti)-half-Skyrmion-(anti)-half-Skyrmion interaction and the half-Skyrmion-anti-half-Skyrmion interaction, the Cooper pairing between holes with the opposite spin states and the opposite half-Skyrmion indices is favorable. Because the interaction between (anti)-half-Skyrmions is repulsive and the interaction between half-Skyrmions and anti-half-Skyrmions is attractive. So we may focus on the pairing correlations described by  $\begin{pmatrix} (-) \\ \mathbf{k};s \end{pmatrix}$ .

At zero temperature, the BCS gap equation is

$$\begin{pmatrix} (-) \\ \mathbf{k};s \end{pmatrix} = \frac{i}{m} \sum_{\mathbf{k} \neq \mathbf{k}^0} \frac{k_x k_y^0 - k_y k_x^0}{(k - k^0)^2} \frac{\begin{pmatrix} (-) \\ \mathbf{k}^0;s \end{pmatrix}}{E_{\mathbf{k}^0}};$$

where  $E_{\mathbf{k}}$  is the quasiparticle excitation energy. This gap equation is divided into two equations according to the relative sign between  $s$  and  $\mathbf{k}$ . For  $\begin{pmatrix} (-) \\ \mathbf{k};s;s \end{pmatrix}$  and  $\begin{pmatrix} (-) \\ \mathbf{k};+ \end{pmatrix}$ , the gap equation is

$$\begin{pmatrix} (-) \\ \mathbf{k};+ \end{pmatrix} = \frac{i}{m} \sum_{\mathbf{k} \neq \mathbf{k}^0} \frac{k_x k_y^0 - k_y k_x^0}{(k - k^0)^2} \frac{\begin{pmatrix} (-) \\ \mathbf{k}^0;+ \end{pmatrix}}{E_{\mathbf{k}^0}}; \quad (1.16)$$

For  $\Delta_{k;s}^{(\pm)}$  and  $\Delta_{k;}^{(\pm)}$ , the gap equation is

$$\Delta_{k;}^{(\pm)} = + \frac{i}{m} \sum_{k' \in k^0} \frac{k_x k_y^0 - k_y k_x^0}{(k - k^0)^2} \frac{\Delta_{k'}^{(\pm)}}{E_{k^0}} : \quad (1.17)$$

Here we consider the case in which both of  $\Delta_{k;+}^{(\pm)}$  and  $\Delta_{k;}^{(\pm)}$  describe the same pairing symmetry. Under this condition, we find  $j_{k;+}^{(\pm)} = j_{k;}^{(\pm)}$  and so  $E_k$  is given by

$$E_k = \sqrt{k^2 + \Delta_{k;+}^{(\pm)2}} = \sqrt{k^2 + \Delta_{k;}^{(\pm)2}} : \quad (1.18)$$

A similar gap equation was analyzed in Ref. 41 in the context of the fractional quantum Hall systems. Following Ref. 41, we introduce an ansatz,

$$\Delta_{k;+}^{(\pm)} = \Delta_k \exp(i\varphi_k) ; \quad (1.19)$$

where  $\varphi$  is an integer and  $\Delta_k = \tan^{-1}(k_y/k_x)$ . Substituting this expression into Eq. (1.16), the integration with respect to the angle  $k^0$  is carried out analytically. At this procedure, we find that there is no solution for  $\varphi = 0$ . Therefore, there is no s-wave pairing state. Furthermore, the gap equation has the solutions only for  $\varphi > 0$ . The gap  $\Delta_k$  satisfies the following equation,

$$\Delta_k = \frac{1}{2m} \sum_{k^0}^Z \Delta_{k^0} \frac{k^0 - k}{E_{k^0}} + \frac{1}{2m} \sum_{k^0}^Z \Delta_{k^0} \frac{k^0 + k}{E_{k^0}} : \quad (1.20)$$

From the asymptotic forms in  $k \rightarrow 1$  and  $k \rightarrow 0$ , we assume the following form for  $\Delta_k$ ,

$$\Delta_k = \begin{cases} \Delta_F & (k=k_F) ; (k < k_F) ; \\ \Delta_F & (k_F=k) ; (k > k_F) ; \end{cases}$$

where  $\Delta_F$  is the Fermi energy of holes and  $k_F$  is the Fermi wave number. The gap is found numerically. The gap decreases by increasing  $\varphi$ . We find  $\Delta_F = 0.916$  for  $\varphi = 1$  and  $\Delta_F = 0.406$  for  $\varphi = 2$ .

The gap equation (1.17) is analyzed similarly. However, because of the sign difference in the interaction the solution has the following form,

$$\Delta_k^{(\pm)} = \Delta_k \exp(i\varphi_k) ; \quad (1.21)$$

where  $\Delta_k$  is the solution of Eq. (1.20). As a result, there are two types of Cooper pairs with opposite relative angular momentum.

For p-wave ( $\varphi = 1$ ) gap symmetry, the sum of  $\Delta_{k;+}^{(\pm)}$  and  $\Delta_{k;}^{(\pm)}$  leads to a  $p_x$ -wave gap which is unstable in the bulk in the absence of symmetry breaking associated with spatial anisotropy. Since s-wave gap symmetry is ruled out as mentioned above, the lowest energy state is obtained for  $d_{x^2-y^2}$ -wave gap symmetry.

The pairing mechanism based on half-Skymions is intuitively understood (Fig. 1.6). According to Eq. (1.10), a half-Skymion, or a gauge flux, is induced

around a hole. If another hole passes the gauge flux region at the Fermi velocity, a magnetic Lorentz-force-like interaction acts on that hole according to the interaction represented by Eq. (1.11). A similar pairing interaction is discussed at half-filled Landau levels.<sup>41,42</sup> In that system the gauge field is the Chern-Simons gauge field<sup>43</sup> whose gauge fluxes cancel the external magnetic field fluxes at the mean field level. Gauge field fluctuations give rise to a pairing interaction between flux attached fermions.

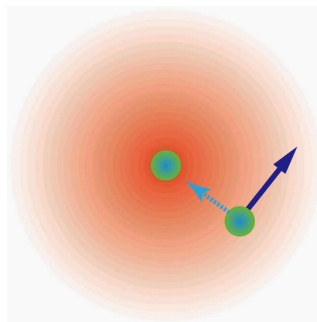


Fig. 1.6. Interaction between doped holes arising from a Berry phase effect associated with the gauge flux created by a half-Skyrmion.

## 1.6. Pseudogap

One of the most intriguing phenomena observed in high-temperature superconductors is the so-called pseudogap which is observed in various physical quantities.<sup>5</sup> Here we focus on the pseudogap behavior observed in ARPES. If the hole concentration is lower than the optimum hole concentration at which the transition temperature is the maximum, the Fermi surface is not a conventional Fermi surface expected from the band theory. Instead, a truncated, an arc-like Fermi surface is observed in ARPES.<sup>6</sup> In order to explain this Fermi arc, a standard approach is to consider a coupling with some boson modes, such as spin fluctuations or gauge field fluctuations associated with phase fluctuations of a mean field, expecting self-energy effects in the single body quasiparticle Green's function. However, it is not obvious that such a conventional analysis leads to qualitatively different physics.

The half-Skyrmion theory provides a completely different approach. To describe the doped hole dynamics which is associated with the spectral function observed by ARPES, we need to include the fact that each doped hole carries a half-Skyrmion. For that purpose, the direct way is to take a doped hole and the half-Skyrmion created by the hole as a composite particle so that the dynamics of the half-Skyrmion is included in the doped hole dynamics.<sup>44</sup>

The Hamiltonian describing the hole hopping is

$$H_t = \sum_{\langle i,j \rangle} \sum_{\sigma} t_{ij} c_{i\sigma}^\dagger c_{j\sigma} + \text{h.c.}; \quad (1.22)$$

where  $t_{ij} = t$  for the nearest neighbor sites,  $t_{ij} = t_1$  for the next nearest neighbor sites, and  $t_{ij} = t_2$  for the third nearest neighbor sites. The parameters  $t_1=t$  and  $t_2=t$  are chosen so that the Fermi surface in the Fermi liquid phase is reproduced.<sup>45</sup>

Now let us include the half-Skyrmion dynamics. The half-Skyrmion dispersion is described by the Hamiltonian,

$$H_{hs} = \sum_{\mathbf{k} \in \text{BZ}} \sum_{\mathbf{R}} \begin{pmatrix} c_{\mathbf{k}+\mathbf{Q}}^\dagger & c_{\mathbf{k}}^\dagger \end{pmatrix} \begin{pmatrix} 0 & v(\cos k_x + \cos k_y) \\ v(\cos k_x - \cos k_y) & 0 \end{pmatrix} \begin{pmatrix} c_{\mathbf{k}} \\ c_{\mathbf{k}+\mathbf{Q}} \end{pmatrix};$$

where the  $\mathbf{k}$ -summation is taken over the reduced Brillouin zone,  $\mathbf{k}_x, \mathbf{k}_y \in [-\frac{\pi}{2}, \frac{\pi}{2}]$ ,  $c_{\mathbf{k}+\mathbf{Q}} = (c_{\mathbf{k}} + c_{\mathbf{k}+\mathbf{Q}})/\sqrt{2}$  and  $c_{\mathbf{k}} = (c_{\mathbf{k}} - c_{\mathbf{k}+\mathbf{Q}})/\sqrt{2}$ , and

$$v = v[(\cos k_x + \cos k_y) + i(\cos k_x - \cos k_y)]:$$

The half-Skyrmion dispersion is given by  $\epsilon_{\mathbf{k}}(\omega)$ . This dispersion corresponds to Eq. (1.7) with  $E_0 = 0$  and  $c_{sw} = v$ . The half-Skyrmion creation energy  $E_0$  is zero because it vanishes in the absence of the antiferromagnetic long-range order.<sup>46</sup> The spin-wave velocity for the doped system is denoted by  $v$  which is different from  $c_{sw}$  in the undoped system. Here we use the same creation operators and the annihilation operators for doped holes and half-Skyrmions. Because a doped hole and the half-Skyrmion carried by the hole is taken as a composite particle. Note that it is not necessary to distinguish between half-Skyrmions and anti-half-Skyrmions. Because their excitation spectra are the same.

The dispersion energy of the composite particle is calculated from  $H = H_t + H_{hs}$  as,

$$E_{\mathbf{k}}(\omega) = \epsilon_{\mathbf{k}}^{(+)}(\omega) + \epsilon_{\mathbf{k}}^{(-)}(\omega);$$

with  $\epsilon_{\mathbf{k}}^{(+)}(\omega) = (\epsilon_{\mathbf{k}} - \epsilon_{\mathbf{k}+\mathbf{Q}})/2$  and  $\epsilon_{\mathbf{k}}^{(-)}(\omega) = 2t(\cos k_x + \cos k_y) - 4t_1 \cos k_x \cos k_y - 2t_2 (\cos 2k_x + \cos 2k_y)$ . The spectral function is calculated following a standard procedure.<sup>47</sup> The imaginary time Green's function for up-spin is defined as

$$G_{\mathbf{k}}(\omega) = \frac{D}{E} T \alpha_{\mathbf{k}}(\omega) c_{\mathbf{k}}^\dagger(0);$$

where  $\alpha_{\mathbf{k}}(\omega) = e^{(\mu - N)} c_{\mathbf{k}} e^{-(\mu - N)}$  with the chemical potential and  $N$  the number operator and  $T$  is the imaginary time ( $\tau$ ) ordering operator.

The Matsubara Green's function is obtained by

$$G_{\mathbf{k}}(i\omega_n) = \frac{Z}{(k_B T)^{-1}} \int_0^{\beta} d\tau e^{i\omega_n \tau} G_{\mathbf{k}}(\tau);$$

where  $\omega_n = (2n+1)k_B T$  ( $n = 0; \pm 1; \pm 2; \dots$ ) is the fermion Matsubara frequency. By the analytic continuation,  $i\omega_n \rightarrow i\omega + 0^+$ , with an infinitesimal positive number,



the retarded Green's function is obtained. Thus, the spectral function is

$$\begin{aligned} A_k(\omega) &= -\frac{1}{\pi} \text{Im} G_k^R(\omega + i0^+) \\ &= \frac{1}{2} (1 + \gamma_k) \delta(\omega - E_k^{(+)} + \gamma_k) + \frac{1}{2} (1 - \gamma_k) \delta(\omega - E_k^{(-)} + \gamma_k); \end{aligned} \quad (1.23)$$

where,

$$\gamma_k = \frac{(2t + v)(\cos k_x + \cos k_y)}{(2t + v)^2 (\cos k_x + \cos k_y)^2 + v^2 (\cos k_x - \cos k_y)^2}.$$

In numerical computations, the parameter  $\gamma_k$  above is taken to be finite so that the  $\delta$ -function in the right hand side of Eq. (1.23) is replaced by the Lorentz function. Figure 1.7 (a) shows  $A_k(\omega = 0)$  with  $\gamma_k = 0.10$ . The resulting Fermi surface is arc-like because the factors  $1 \pm \gamma_k$  suppress the intensity in part of the Brillouin zone. This arc-like Fermi surface is consistent with the ARPES results.

However, there is some deviation from the experiment around the ends of the arc.<sup>48</sup> Basically the Fermi arc follows the underlying Fermi surface which appears at high-temperature above the characteristic pseudogap temperature,  $T^*$ . The deviation is suppressed by including the effect of the short-range antiferromagnetic correlation.<sup>49,50</sup> The effect is included by taking average over the wave vector change in the (incommensurate) antiferromagnetic correlation. The calculation is similar to that described in Ref. 49. Figure 1.7 (b) shows how the spectral intensity is modified at the antiferromagnetic correlation length  $\lambda_{AF} = 10$ .

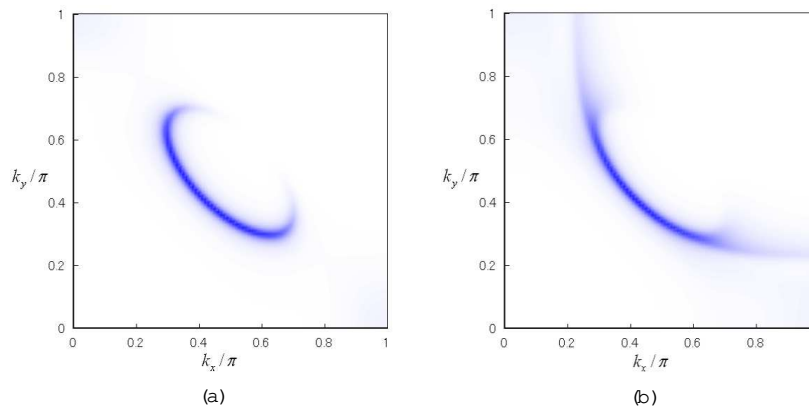


Fig.1.7. (a) The intensity plot of the spectral function  $A_k(\omega = 0)$  in a quadrant of the Brillouin zone. The doping concentration is  $x = 0.10$ . The other parameters are  $t_1 = t = 0.25$ ,  $t_2 = t = 0.10$ , and  $v = t = 1.0$ . (b) The intensity plot of the spectral function  $A_k(\omega = 0)$  with including the effect of the short-range antiferromagnetic correlation. The antiferromagnetic correlation length is taken as  $\lambda_{AF} = 10$ .

Now we comment on the similarity to the d-density wave theory.<sup>13</sup> The calculation for the spectral function  $A_k(\omega)$  is almost identical to that in the d-density

wave theory.<sup>51</sup> However, the physical interpretation of  $v$  is different. In  $d$ -density wave theory,  $v$  is associated with  $d$ -density wave long-range order. But here  $v$  is associated with the half-Skym ions dynamics. Although the origin is different, the half-Skym ion theory and the  $d$ -density wave theory may share some results about the pseudogap phenomenon because the Hamiltonian is almost the same.

### 1.7. Summary

In this chapter, we have reviewed the half-Skym ion theory for high-temperature superconductivity. We have mainly focused on four topics. First, we have discussed the single hole doped system. The correlation of forming a singlet state between a doped hole spin and a copper spin has been investigated including the fact that the hole wave function extends over a space, and affected by the other copper site spins. A half-Skym ion spin texture created by a doped hole has been described. It is shown that the half-Skym ion excitation spectrum is in good agreement with the ARPES results in the undoped system.

The most important aspect of the half-Skym ion is that the doped hole carries a topological charge which is represented by a gauge flux in the  $CP^1$  representation. This property is in stark contrast to conventional spin polaron pictures. Because in that case interaction clouds arising from spin correlations are not characterized by a topological charge or a gauge flux.

Second, we have considered multi-half-Skym ion configurations. In multi-half-Skym ion configurations, antiferromagnetic long-range order is suppressed around the doping concentration,  $x = 0.10$ . The topological property of half-Skym ions is kept for  $x < 0.30$  as shown by numerical simulations. After suppression of antiferromagnetic long-range order, the spin correlation becomes incommensurate. Numerical simulations suggest that the origin of the incommensurate spin correlation is associated with stripe configurations of half-Skym ions and anti-half-Skym ions.

Third, we have discussed a mechanism of  $d_{x^2-y^2}$ -wave superconductivity. The gauge flux created by half-Skym ions induces the interaction between doped holes. The interaction leads to a  $d_{x^2-y^2}$ -wave superconducting state of doped holes. The origin of the attractive interaction is a Lorentz force acting on a hole moving in a gauge flux created by another hole.

Finally, we have discussed a pseudogap phenomenon. We have considered a composite particle of a hole and half-Skym ion. The pseudogap is associated with the excitation spectrum of the composite particle.

Although several aspects of the half-Skym ion theory for high-temperature superconductivity are described in this review, we need further studies to establish the theory. In particular it is necessary to show the half-Skym ion formation in the single hole doped system in a more convincing way to provide a sound starting point.

## Acknowledgements

I would like to thank T. Tohyama and G. Baskaran for helpful discussions. This work was supported by the Grant-in-Aid for Scientific Research from the Ministry of Education, Culture, Sports, Science and Technology (MEXT) of Japan, the Global COE Program "The Next Generation of Physics, Spun from Universality and Emergence," and Yukawa International Program for Quark-Hadron Sciences at YITP. The numerical calculations were carried out in part on Altix3700 BX2 at YITP in Kyoto University.

## References

1. J. G. Bednorz and K. A. Müller, Possible high  $T_c$  superconductivity in the Ba-La-Cu-O system, *Z. Phys. B: Condens. Matter.* 64 (2), 189{93, (1986).
2. M. Imada, A. Fujimori, and Y. Tokura, Metal-insulator transitions, *Rev. Mod. Phys.* 70 (4), 1039{1263, (1998).
3. D. J. Van Harlingen, Phase-sensitive tests of the symmetry of the pairing state in the high-temperature superconductors (Evidence for  $d_{x^2-y^2}$  symmetry), *Rev. Mod. Phys.* 67 (2), 515{535, (1995).
4. E. Manousakis, The spin- $\frac{1}{2}$  Heisenberg antiferromagnet on a square lattice and its application to the cuprous oxides, *Rev. Mod. Phys.* 63 (1), 1{62, (1991).
5. T. Timusk and B. W. Statt, The pseudogap in high-temperature superconductors: an experimental survey, *Rep. Prog. Phys.* 62 (1), 61{122, (1999).
6. M. R. Norman, H. Ding, M. Randeria, J. C. Campuzano, T. Yokoya, T. Takeuchi, T. Takahashi, T. Mochiku, K. Kadowaki, P. Guptasarma, and D. G. Hinks, Destruction of the Fermi surface underdoped high- $T_c$  superconductors, *Nature.* 392, 157{160, (1998).
7. A. Damascelli, Z. Hussain, and Z. X. Shen, Angle-resolved photoemission studies of the cuprate superconductors, *Rev. Mod. Phys.* 75 (2), 473, (2003).
8. C. Renner, B. Revaz, J.-Y. Genoud, K. Kadowaki, and J. Fischer, Pseudogap precursor of the superconducting gap in under- and overdoped  $Bi_2Sr_2CaCu_2O_{8+x}$ , *Phys. Rev. Lett.* 80 (1), 149{152, (1998).
9. F. C. Zhang and T. M. Rice, Effective Hamiltonian for the superconducting Cu oxides, *Phys. Rev. B.* 37 (7), 3759{3761, (1988).
10. P. A. Lee, N. Nagaosa, and X. G. Wen, Doping a Mott insulator: Physics of high-temperature superconductivity, *Rev. Mod. Phys.* 78 (1), 17{85, (2006).
11. P. W. Anderson, The resonating valence bond state in  $La_2CuO_4$  and superconductivity, *Science.* 235, 1196{1198, (1987).
12. S. A. Kivelson, I. P. Bindloss, E. Fradkin, V. O. Ganesyan, J. M. Tranquada, A. Kapitulnik, and C. Howald, How to detect fluctuating stripes in the high-temperature superconductors, *Rev. Mod. Phys.* 75 (4), 1201{1241, (2003).
13. S. Chakravarty, R. B. Laughlin, D. K. Morr, and C. Nayak, Hidden order in the cuprates, *Phys. Rev. B.* 63 (9), 094503, (2001).
14. D. P. Arovas and A. Auerbach, Functional integral theories of low-dimensional quantum Heisenberg models, *Phys. Rev. B.* 38 (1), 316{332, (1988).
15. J. E. Hirsch and S. Tang, Comment on a mean-field theory of quantum antiferromagnets, *Phys. Rev. B.* 39 (4), 2850{2851, (1989).

16. D. Yoshioka, Boson mean field theory of the square lattice Heisenberg model, *J. Phys. Soc. Jpn.* 58, 3733{3745, (1989).
17. M. Raykin and A. Auerbach,  $1/N$  expansion and long range antiferromagnetic order, *Phys. Rev. Lett.* 70 (24), 3808{3811, (1993).
18. A. Fetter and J. Walecka, *Quantum Theory of Many-Particle Systems*. (Courier Dover Publications, 2003).
19. S. Chakravarty, B. I. Halperin, and D. R. Nelson, Low-temperature behavior of two-dimensional quantum antiferromagnets, *Phys. Rev. Lett.* 60 (11), 1057{1060, (1988).
20. R. J. Gooding, Skyrmion ground states in the presence of localizing potentials in weakly doped  $\text{CuO}_2$  planes, *Phys. Rev. Lett.* 66 (17), 2266{2269, (1991).
21. S. Haas, F.-C. Zhang, F. Mila, and T. M. Rice, Spin and charge texture around in-plane charge centers in the  $\text{CuO}_2$  planes, *Phys. Rev. Lett.* 77 (14), 3021{3024, (1996).
22. A. A. Belavin and A. M. Polyakov, Metastable states of two-dimensional isotropic ferromagnets, *JETP Lett.* 22 (10), 245{248, (1975).
23. R. Rajaraman, *Solitons and instantons*. (North-Holland, 1987).
24. T. K. Ng, Topological spin excitations of Heisenberg antiferromagnets in two dimensions, *Phys. Rev. Lett.* 82 (17), 3504{3507, (1999).
25. T. Morinari, Half-skyrmion picture of a single-hole-doped  $\text{CuO}_2$  plane, *Phys. Rev. B.* 72, 104502, (2005).
26. B. O. Wells, Z. X. Shen, A. Matsura, D. M. King, M. A. Kastner, M. G. Reven, and R. J. Birgeneau, E versus  $k$  relations and many-body effects in the model insulating copper-oxide  $\text{Sr}_2\text{CuO}_2\text{Cl}_2$ , *Phys. Rev. Lett.* 74 (6), 964{967, (1995).
27. B. B. Beard, R. J. Birgeneau, M. G. Reven, and U. Wiese, Square-lattice Heisenberg antiferromagnet at very large correlation lengths, *Phys. Rev. Lett.* 80 (8), 1742{1745, (1998).
28. J.-K. Kim and M. Troyer, Low temperature behavior and crossovers of the square lattice quantum Heisenberg antiferromagnet, *Phys. Rev. Lett.* 80 (12), 2705{2708, (1998).
29. R. R. P. Singh, Thermodynamic parameters of the  $T = 0$ , spin-1/2 square-lattice Heisenberg antiferromagnet, *Phys. Rev. B.* 39 (13), 9760{9763, (1989).
30. T. Morinari, Strong-coupling analysis of QED<sub>3</sub> for excitation spectrum broadening in the undoped high-temperature superconductors, *Phys. Rev. B.* 77 (7), 075128, (2008).
31. M. Berciu and S. John, Magnetic structure factor in cuprate superconductors: Evidence for charged meron vortices, *Phys. Rev. B.* 69 (22), 224515, (2004).
32. S. I. Belov and B. I. Kochelaev, Nuclear spin relaxation in two-dimensional Heisenberg antiferromagnet  $S = 1/2$  with skyrmions, *Solid State Commun.* 106 (4), 207 { 210, (1998).
33. C. Timm and K. H. Bennemann, Doping dependence of the Neel temperature in Mott-Hubbard antiferromagnets: Effect of vortices, *Phys. Rev. Lett.* 84 (21), 4994{4997, (2000).
34. S.-W. Cheong, G. Aeppli, T. E. Mason, H. Mook, S. M. Hayden, P. C. Canfield, Z. Fisk, K. N. Clausen, and J. L. Martinez, Incommensurate magnetic fluctuations in  $\text{La}_2 \times \text{Sr}_x \text{CuO}_4$ , *Phys. Rev. Lett.* 67 (13), 1791{1794, (1991).
35. K. Yamada, C. H. Lee, K. Kurahashi, J. Wada, S. Wakimoto, S. Ueki, H. Kimura, Y. Endoh, S. Hosoya, G. Shirane, R. J. Birgeneau, M. G. Reven, M. A. Kastner, and Y. J. Kim, Doping dependence of the spatially modulated dynamical spin correlations and the superconducting-transition temperature in  $\text{La}_2 \times \text{Sr}_x \text{CuO}_4$ , *Phys. Rev. B.* 57 (10), 6165{6172, (1998).
36. M. Matsuda, M. Fujita, K. Yamada, R. J. Birgeneau, M. A. Kastner, H. Hiraka, Y. Endoh, S. Wakimoto, and G. Shirane, Static and dynamic spin correlations in the spin-glass phase of slightly doped  $\text{La}_2 \times \text{Sr}_x \text{CuO}_4$ , *Phys. Rev. B.* 62 (13), 9148{9154,

- (2000).
37. T. Morinari, Mechanism of  $d_{x^2-y^2}$ -wave superconductivity based on hole-doping-induced spin texture in high  $T_c$  cuprates, *Phys. Rev. B* . 73 (6), 064504, (2006).
  38. T. Morinari, Mechanism of unconventional superconductivity induced by skyrmion excitations in two-dimensional strongly correlated electron systems, *Phys. Rev. B* . 65 (6), 064513, (2002).
  39. B. I. Shraiman and E. D. Siggia, Mobile vacancies in a quantum Heisenberg antiferromagnet, *Phys. Rev. Lett.* 61 (4), 467{470, (1988).
  40. M. Sigrist and K. Ueda, Phenomenological theory of unconventional superconductivity, *Rev. Mod. Phys.* 63 (2), 239{311, (1991).
  41. M. Greiter, X. G. Wen, and F. Wilczek, Paired Hall states, *Nucl. Phys. B* . 374 (3), 567{614, (1991).
  42. T. Morinari, Composite fermion pairing theory in single-layer systems, *Phys. Rev. B* . 62 (23), 15903{15912, (2000).
  43. S.-C. Zhang, The Chern-Simons-Landau-Ginzburg theory of the fractional quantum Hall effect, *Int. J. Mod. Phys. B* . 6 (1), 25{58, (1992).
  44. T. Morinari, Fermion formation by chiral spin textures in high-temperature superconductors, *J. Phys. Chem. Solids* . 69 (12), 2690{2692, (2008).
  45. T. Tohyama and S. Masekawa, Angle-resolved photoemission in high  $T_c$  cuprates from theoretical viewpoints, *Supercond. Sci. Technol.* 13 (4), R17{R32, (2000).
  46. A. Auerbach, B. E. Larson, and G. N. Murthy, Landau-level spin waves and Skyrmion energy in the two-dimensional Heisenberg antiferromagnet, *Phys. Rev. B* . 43 (13), 11515{11518, (1991).
  47. A. A. Abrikosov, L. P. Gor'kov, and I. Dzyaloshinskii, *Methods of Quantum Field Theory in Statistical Physics*. (Pergamon, New York, 1965).
  48. M. R. Norman, A. Kanigel, M. Randeria, U. Chatterjee, and J. C. Camuzano, Modeling the fermion in underdoped cuprates, *Phys. Rev. B* . 76, 174501, (2007).
  49. N. Harrison, R. D. McDonald, and J. Singleton, Cuprate fermion orbits and fermion arcs: The effect of short-range antiferromagnetic order, *Phys. Rev. Lett.* 99 (20), 206406, (2007).
  50. T. Morinari, Pseudogap and short-range antiferromagnetic correlation controlled fermion surface in underdoped cuprates: From fermion arc to electron pocket, *arXiv*: 0805.1977. (2008).
  51. S. Chakravarty, C. Nayak, and S. Tewari, Angle-resolved photoemission spectra in the cuprates from the d-density wave theory, *Phys. Rev. B* . 68 (10), 100504 (R), (2003).